



Effect of multi-walled carbon nanotubes on the performance evaluation of nickel-based super-alloy–Udimet 720 machined using WEDM process

Rakesh Chaudhari¹ · Izaro Ayesta² · Mikesh Doshi¹ · Sakshum Khanna¹ · Vivek K. Patel¹ · Jay Vora¹ · Luis Norberto López De Lacalle²

Received: 5 August 2022 / Accepted: 25 September 2022 / Published online: 26 October 2022
© The Author(s) 2022

Abstract

The diverse capabilities of nickel-based super-alloy (Udimet 720), like robust mechanical strength, ductility, resistance to excessive temperature deformation, and advanced corrosion and oxidation resistance, make it suitable for use in multiple applications. These super-alloys are identified as extremely difficult materials for machining to meet feature and manufacturing requirements. In the present work, we demonstrated the machining of Udimet 720 by employing the wire-electrical discharge machining (WEDM) technique. Pulse-on-time (T_{on}), pulse-off-time (T_{off}), current, and MWCNT amount were preferred as input variables. The effect of selected design variables was studied on material removal rate (MRR), surface roughness (SR), and recast layer thickness (RLT). Box-Behnken design was utilized to design an experimental matrix. For statistical analysis, analysis of variance (ANOVA) was employed. From ANOVA, the current had the highest contributor with 35.85% to affect MRR, while MWCNT amount was found to be the highest contributor for deciding the values of both SR and RLT with contributions of 42.66% and 40.07%, respectively. The addition of MWCNT at 1 g/L has substantially improved MRR from 0.8546 to 1.2199 g/min, SR reduced from 5.88 μm to 2.98 μm , and reduction in RLT from 17.8 to 11.61 μm . The passing vehicle search (PVS) algorithm was implemented, and the results of single-objective optimization presented the largest MRR of 1.8883 g/min, least SR of 1.89 μm , and least RLT of 9.70 μm . Additionally, a set of non-dominated solutions was obtained through Pareto optimal fronts. A small acceptable deviation was detected among the actual and forecasted results from PVS algorithm. It clearly reveals the acceptance of the PVS technique in the present study for Udimet 720. Lastly, the significance of MWCNT amount on surface textures was revealed by employing scanning electron microscopy (SEM).

Keywords Nickel-based super-alloy · Udimet 720 · MWCNTs · Optimization · Passing vehicle search algorithm · WEDM

1 Introduction

The history of super-alloy and the development of novel alloy mixtures and methods were treated as improvements during World War II of 1940. It is an excellent project that

makes utilization of military plane engines. Super-alloys are used nowadays because they meet high standards for durability and strength requirements [1]. A super-alloy is a strong mixture that is utilized in high-temperature applications. The diverse capabilities consist of robust mechanical strength,

✉ Izaro Ayesta
izaro.ayesta@ehu.es

✉ Jay Vora
jay.vora@sot.pdpu.ac.in

Rakesh Chaudhari
rakesh.chaudhari@sot.pdpu.ac.in

Mikesh Doshi
mikesh.dmtmm20@sot.pdpu.ac.in

Sakshum Khanna
sakshum.khanna@gmail.com

Vivek K. Patel
vivekp@sot.pdpu.ac.in

Luis Norberto López De Lacalle
norberto.lzlacalle@ehu.es

¹ School of Technology, Pandit Deendayal Energy University, Gandhinagar 382007, Gujarat, India

² Department of Mechanical Engineering, University of the Basque Country, Escuela Superior de Ingenieros Alameda de Urquijo S/N, 48013 Bilbao, Spain

ductility, resistance to excessive temperature deformation, and advanced corrosion and oxidation resistance [2]. Surface integrity issues are critical in this regard whenever introducing a novel super-alloy [3, 4]. They are used in a variety of sectors, including aviation parts and components, automobile parts, the pharmaceutical sector, spacecraft components, nuclear power systems, steam plants, and the chemical industry [5]. Nickel-based, iron-based, and cobalt-based are the three types of super-alloys. Face-centered cubic (FCC) structure, solid solution precipitation enhancement, and topologically close phase (TCP) are characteristics of Ni-based super-alloys. They are usually utilized at temperatures ranging from 1200 to 1500 °C. Alloying elements in high concentrations offer strength, hardness, and durability. At the same time, changes in composition, heat treatment, and increased temperature may all be used to influence the characteristics of super-alloys [6]. The introduction of the strengthening phase precipitates strengthens the super-alloys. An austenitic structure in nickel-base super-alloys has an extended solubility for specific alloying additives and adequate characteristics to support the establishment of a particularly effective strengthening phase [7]. Ni-based super-alloys have ductility, higher cohesive energy, thermally induced creep, and a low diffusion coefficient [8]. Nickel-based super-alloys are identified as extremely difficult materials for machining to meet feature and manufacture requirements [9]. The nickel-based super-alloys machining is challenging owing to low heat conductivity, work hardening propensity, and high strength [10, 11].

Super-alloys based on nickel, such as Udimet 720, play a vital role in the aerospace sector, accounting for more than half of the capacity of gas turbine airplanes. Udimet 720 has outstanding fatigue, corrosion, mechanical, and heat resistance, making it perfect for usage in harsh environments. With high strength and corrosion resistance, Udimet 720 is typically used on the turbine portion of the motor, where temperature changes can reach 1650 K due to its ability to sustain high strength at higher temperatures [12]. Because of their extreme molecular affinity for many tooling materials, rapid stress hardening rates, and comparatively limited thermal conductivity, Udimet 720 is difficult to machine. Owing to this restricted machinability, obtaining the high degree of surface quality required by the aviation industry may be expensive and time-consuming [13].

Machining of Udimet 720 is very difficult due to rapid tool life and undesirable machined surface. Traditional machining of nickel-based alloys is regarded as a poor choice owing to their lower thermal conductivity [14]. Lower conductivity increases to the emergence of heating among tool and work components, larger wear, and a higher occurrence of the chemical reaction by the cutting substance creating the machining process more challenging [15]. Recent studies show that standard machining techniques for modern

engineering materials, including Udimet 720, are often difficult owing to higher strength, hardness, and considerable heat generation [16]. Furthermore, conventional machining reduces the tool life owing to lower heat conductivity [17]. Another limitation of conventional machining for Udimet 720 is the poor surface finish, poor dimensional accuracy, noise operation, and difficulty in producing complex shape geometries. As a result, the non-traditional machining method is largely suitable for machining Udimet 720.

The wire electrical discharge machining (WEDM) process is largely utilized to process difficult-to-cut materials. WEDM process makes use of thermal energy to erode the material from the base material [18, 19]. WEDM technique is largely suitable to obtain enhanced performances for high strength and high hardness materials [20]. WEDM is known for obtaining intricate forms. Thermal energy generated during the process creates excessive temperature sparks [21]. These high-temperature sparks are then used to erode material by melting and vaporization [22]. The generation of higher temperature between tool and base material creates several defects on the machined surfaces, poor surface quality, debris deposition, formation of cracks and pores, and the development of recast layer thickness (RLT) [23, 24]. Therefore, it becomes necessary to find a suitable approach for the removal of these surface irregularities of the machined product [25]. In addition to surface irregularities, material removal rate (MRR) becomes crucial in any machining process for obtaining higher productivity [26]. As a result, simultaneous improvement in obtaining higher MRR and minimizing the SR and RLT are essential. This can be achieved by adding suitable nanopowder during machining [27]. Many researchers have observed a considerable rise in thermal conductivity and improvements in surface quality by adding the appropriate amount of nanopowders in the dielectric [28]. Various nanopowders were utilized to create nano-fluids for the improvement of machined surfaces [29]. Nanopowder properties like conductivity, size and density become important for performance [30]. Recently, a large number of researchers have used carbon-based nanostructures to produce nano-fluids, such as single-walled carbon nanotubes (SWNTs), graphite, and multi-walled carbon nanotubes (MWNTs). MWCNTs were observed to have outstanding electrical and mechanical properties along with large thermal conductivity [31]. Therefore, dielectric fluid containing nanotubes/grapheme sheets is expected to have better thermal conductivity and enhance the machining performance and surface quality [32]. MWCNTs increase the processing performance along with the reduction in micro-cracks on the treated surface. MWCNTs are favored over SWCNTs because they have several concentric graphene layers, which results in enhanced chemical and thermal stability [33]. Increased corrosion resistance and strength are two additional advantages of MWCNTs and they are less prone

to oxide formation than SWCNTs [34]. The cost of processing MWCNTs is the same as the cost of mass manufacture.

The WEDM process consists of various input and output parameters. Controlling these parameters plays a vital role, especially in a process where a conflicting situation arises among the response variables. Several multi-response optimization methods were employed during machining to accomplish multiple objectives simultaneously. Passing vehicle search (PVS) is one such technique that has proved to be reasonably effective, especially for engineering problems. PVS algorithm is a meta-heuristic optimization method that uses the vehicle's passing behavior. It acts as a human activity-based technique. The PVS algorithm finds the global or near-optimal solutions for specified objective functions. Past studies suggest that the PVS algorithm was effectively employed in the EDM process to attain desired multi-response optimal solution [35]. Parsan et al. [36] used the PVS algorithm for EDM of Mg-RE-Zn-Zr alloy. They articulated a regression model for the selected responses. Obtained results suggest that the PVS algorithm was very beneficial for Pareto fronts as well as optimized results. Comparative analysis of the PVS algorithm with other algorithms suggests that optimization results from the PVS algorithm give more accuracy than different approaches [37].

Antar et al. [12] used the WEDM process to minimize the workpiece damage for Udimet 720. They have compared the machined surface obtained through the WEDM process with milled specimens. Their results reveal that the WEDM process is widely suitable for manufacturing complex aerospace components. Singh and Garg [38] used T_{on} , T_{off} , SV, and current as input variables for the WEDM process with the response of MRR. They anticipated that the ideal selection of process parameters would optimize the MRR. MRR was increased with the rise in T_{on} and current, while it decreased with rising in T_{off} and SV. Soni et al. [39] preferred WEDM machining for nickel-based super-alloy (Ti50Ni40Co10) to enhance the performance of MRR and SR. Increasing T_{on} and decreased value of T_{off} and SV has improved both responses. Obtained results have shown that T_{on} lower than 125 μ s would be helpful in the minimization of micro-crack and RLT. Jadam et al. [32] used MWCNT amount in the dielectric fluid to investigate nickel-based super-alloys EDM performance. The effect of current was also studied along with the MWCNT amount. With the MWCNT amount, MRR was observed to be enhanced by 44.95%, TWR reduced by 64.1%, and SR reduced by 14.1% compared to normal EDM, i.e., without MWCNT amount. Apart from this, surface defects were also minimized at 0.5 g/L of MWCNT amount, owing to the excellent conductivity of MWCNT in the inter-electrode gap (IEG). Peças and Henriques [40] compared the obtained results from Si powder-mixed EDM with conventional EDM. Obtained results have shown a substantial reduction in RLT and SR. They concluded that the

proper concentration of nanopowder improves machining performance. The machining abilities of the EDM process have been enhanced by using CNTs combined with dielectric fluid by Shabgard and Khosrozadeh [41] for Ti6Al4V alloy. The machined surface was investigated using SEM, and obtained results have shown a significant reduction of micro-cracks due to the mixing of CNTs in a dielectric.

Additionally, MWCNT also enhanced the machining performance by reducing the TWR as well as SR. Dresselhaus et al. [42] reported that CNTs demonstrate excellent thermal and electrical properties of CNTs. These properties can be efficiently used to improve EDM performances. Izman et al. [43] compared the EDM performance by adding MWCNT into kerosene dielectric fluid with the conventional EDM process. With the use of MWCNT amount, MRR was observed to be enhanced by 7%, and SR reduced by 9% as compared to the normal EDM process. RLT was also observed to be reduced with the use of MWCNT amount. Prabhu and Vinayagam [44] used CNT mixed dielectric fluid to improve the EDM process's machining performance for Inconel 718. Their results revealed that the use of CNT has improved surface characteristics by means of reduction in micro-cracks, globules, and SR. Chaudhari et al. [45] implemented varying concentrations of MWCNT amount for WEDM of Nitinol along with other input parameters of T_{on} , T_{off} , and current as input parameters. Their results have shown an improvement of 75.42% for MRR and 19.15% for SR at 1 g/L amount of MWCNT as compared to WEDM process. Additionally, a considerable drop in surface defects was achieved by using the MWCNT amount at 1 g/L.

The studied literature has shown that the effect of MWCNT on WEDM machining of Udimet 720 has not been discovered. However, as per our author's understanding, multi-response optimization by employing the PVS algorithm and investigation of MWCNT nanopowder is not yet conveyed for nickel-based super-alloy-Udimet 720 with the WEDM process. The present study narrowed the research gap, and work on the machinability of Udimet 720 was conducted. In the present study, T_{on} , T_{off} , current, and MWCNT amounts were preferred as input parameters. The effect of selected design variables was studied on MRR, SR, and RLT. Box-Behnken's design of RSM has been utilized to prepare the sequence of experimental trials. Analysis of variance (ANOVA) was employed to investigate the statistical analysis. PVS algorithm was implemented, and the results of single-objective optimization presented the largest MRR of 1.8883 g/min, least SR of 1.89 μ m, and least RLT of 9.70 μ m. Additionally, a set of non-dominated solutions was obtained through Pareto optimal fronts. A slight acceptable deviation was detected among the actual and forecasted results from the PVS algorithm. It clearly reveals the acceptance of the PVS technique in the present study for Udimet 720. Lastly, the significance of MWCNT amount on surface textures was

revealed by employing scanning electron microscopy (SEM). The authors believe that the present study will be largely beneficial for industrial applications.

2 Materials and methods

2.1 Preparation of MWCNT

As per our previous study, multi-wall carbon nanotubes (MWCNT) were prepared to utilize a modified hydrothermal technique [45]. NaOH, anhydrous C_2H_5OH , and PEG were required as essential components in the synthesis of multi-wall carbon nanotube. The MWCNT was created by rapidly stirring 8 g NaOH and 4 g PEG in an ethanol and water (16:2) combination for 1.15 h. After mixing, the liquid was placed in an autoclave and sealed. The studies were carried out in a furnace at a variety of temperatures, including 120 °C, 160 °C, and 200 °C, for 18 h before being naturally cooled down to room temperature in 6 h. The resulting material was centrifuged and washed three to four times in ethyl alcohol and DI water. The samples were then dried for 10 h at 75 °C. The surface structure and morphological properties of as-prepared MWCNTs were examined by FESEM (Model: ULTRA 55, Company: Carl Zeiss) and micro-Raman spectroscopy (Model: In Via Raman microscope, Company: Renishaw with 532 nm Argon laser).

2.2 Experimental plan

For the current experimentations, a nickel-based super-alloy known as Udimet 720, molybdenum, MWCNT, and EDM oil as dielectric fluid was considered as work material tool wire, powder, and dielectric, respectively. Table 1 displays the chemical composition for Udimet 720. The density of as-received Udimet 720 was observed to be 8.08 g/cc. In the present study, T_{on} , T_{off} , current, and MWCNT amounts were chosen as variables from the results of pilot experiments, the capability of setup, and studied literature. The machining conditions used in the present work are represented in Table 2. The influence of designated parameters was studied on MRR, SR, and RLT. Rectangular slots were cut from work material Udimet 720 by using experimental runs obtained by Box-Behnken design (BBD). BBD employs the RSM technique to get an optimal response by proper arrangement of the experimental runs [46]. It minimizes the number of runs and saves additional cost and effort [47].

Table 2 Machining conditions

Process parameter	Levels
Pulse-on time, T_{on} (μ s)	25; 50; 75
Pulse-off time, T_{off} (μ s)	6; 12; 18
Discharge current (A)	2; 4; 6
MWCNTs (g/L)	0; 0.5; 1
Nanopowder	MWCNT
Nanopowder size (nm)	10–20

The amount of material removal in g/min was determined through Eq. (1).

$$MRR = \frac{\Delta W}{t} \quad (1)$$

where ΔW represents eroded material in gram, t depicts the time in minutes.

Surftest-410 was employed to determine the SR of experimental components. SR was determined at multiple places, and their average reading was taken for examination. Measurement of RLT and analysis of surface were carried out by using FESEM.

2.3 PVS optimization

Savsani and Savsani [37] proposed the PVS algorithm, which has proved to be reasonably effective, especially for engineering design problems. The philosophy of this algorithm is that it imitates the mechanism of a passing vehicle on a two-lane highway. Here, the primary principle of a safe overtaking opportunity has been considered. The mechanism depends on several interdependent yet complex parameters, namely gap availability in traffic coming from the opposite side, acceleration and speed of individual vehicles, the overall traffic, driver skill, weather, and road conditions. The algorithm reflects 3 types of vehicles (namely back-vehicle (BV), front-vehicle (FV), and oncoming-vehicle (OV)) on two-lane highways. Suppose if BV desires to overtake FV, then it is essential to have a higher speed of BV than FV. Overtaking of BV will not occur if BV has less speed than FV. Additionally, overtaking would also depend on the speed and position of OV and the distance between them, along with their velocities.

Assuming that three different vehicles (BV, FV, and OV) on a two-lane highway have different velocities (V_1 , V_2 , and V_3), x is the distance between BV and FV, and y is the distance between FV and OV at any particular time instance. Two

Table 1 Chemical composition of Udimet 720

Element	Ni	Cr	Co	Mo	Ti	Al	W
Wt. %	55.16–59.705	15.5–16.5	14–15.5	2.75–3.25	4.75–5.25	2.25–2.75	1.0–1.5

primary conditions resulting from the FV and BV velocity would be that FV is slower than BV ($V_1 > V_3$) and vice versa. If FV is faster than BV, passing is not possible, and BV would be able to move with the desired velocity. Possibility of passing only occurs if FV is slower than BV. One additional condition for the situation is that passing is possible only if the distance from FV at which passing occurs is less than the distance covered by OV. Thus, several different conditions arise for those selected vehicles. The present study employed the PVS algorithm, effectively solving various engineering problems. PVS algorithm is a meta-heuristic optimization method that uses the vehicle's passing behavior. It acts as a human activity-based technique. The PVS algorithm finds the global or near-optimal solutions for specified objective functions.

3 Results and discussion

3.1 Analyses of MWCNT

MWCNT morphology was investigated by SEM technique (Fig. 1a). The micrographs indicate the production of elongated and even tubular carbon nanostructures resembling nanotubes. The SEM can also see inside different nano tubular structures with average lengths and diameters of roughly 5–10 μm and 10–20 nm, respectively. Furthermore, as shown in Fig. 1, the structural characterization of several MWCNTs manufactured at various temperatures was executed using Raman spectroscopy (b). A specific peak of graphitic bands was identified in as-prepared MWCNT samples at 1590 cm^{-1} , with a shoulder peak at 1764 cm^{-1} , which can be attributed to the C–C bond in-plane vibration known as the G band. A peak at 1361 cm^{-1} was also observed, indicating flaws and disorder in carbon systems (D band). The G band, which is the D band's overtone, is responsible for the peak at 2695 cm^{-1} . The creation of nanotubes occurs as the hydrothermal temperature rises, according to the diffraction peaks recorded for diverse samples. When comparing the sample

hydrothermal to various temperatures, the greatest intensity was seen at 160°C , confirming complete MWCNT production. Thus, the production of MWCNT for further treatment and characterization process was carried out at an optimized temperature of 160°C for 24 h. Furthermore, X-ray diffraction spectroscopy was carried out for all MWCNT samples synthesized at different temperatures, as shown in Fig. 1a. The peaks at 25.19° , 43.18° , 55.42° , and 78.19° correspond to the (002), (100), (004), and (101) planes, respectively (JCPDS No. 23–64), with P63/MMC. The diffractogram peaks detected for several samples revealed that the production of nanotubes happens as the hydrothermal temperature rises. Furthermore, raising the temperature above 160°C causes additional disordered phases of MWCNT to form, lowering the peak's intensity and boarding. As a result, the pattern confirms the production of wurtzite-structured carbon tubes in a cylindrical shape.

3.2 ANOVA for responses

Table 3 depicts the results of experimental runs prepared from the BBD method at varying values of design variables. Figure 2 depicted the machined specimens as per the L27 design of BBD. To understand the relationship between the parameters and responses, mathematical correlations were generated through BBD design for all responses. For validation of generated models and to apprehend the impact of variables through statistical analysis, ANOVA was employed through Minitab v17. The confidence level of 95% was taken for the assessment of variables for responses about their contributions. For this purpose, the selected response must have a *P*-value of a particular variable lower than 0.05 [48].

Significant model terms were identified using the ANOVA statistical analysis for the measured response values. ANOVA for MRR was depicted in Table 4. Model *f*-value of 8.28 with a smaller *P*-value concluded the complete significance of the model. In addition, linear model terms including all WEDM process variables (T_{on} , T_{off} ,

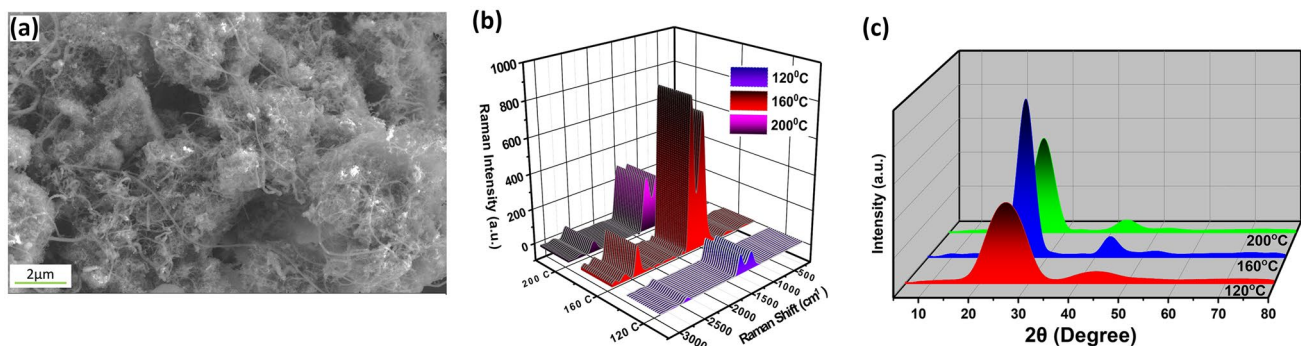


Fig. 1 a SEM of MWCNT; b Raman profile; c XRD spectra of multi-wall carbon nanotubes synthesized at various temperatures for 24 h

Table 3 L27 design as per BBD and response readings

Std. order	Run order	T_{on} (μ s)	T_{off} (μ s)	Current (A)	MWCNT (g/L)	MRR (g/min)	SR (μ m)	RLT (μ m)
15	1	50	6	6	0.5	1.66234	6.225	19.90
10	2	75	12	4	0.0	0.81501	7.245	21.00
16	3	50	18	6	0.5	1.23146	3.705	13.90
27	4	50	12	4	0.5	1.33791	4.260	14.00
9	5	25	12	4	0.0	0.84018	4.020	13.05
20	6	75	12	6	0.5	1.58179	5.910	19.10
24	7	50	18	4	1.0	1.10323	2.505	10.35
17	8	25	12	2	0.5	0.48020	2.970	12.15
23	9	50	6	4	1.0	1.52218	3.900	13.40
13	10	50	6	2	0.5	1.08960	5.130	15.45
5	11	50	12	2	0.0	0.99579	5.415	16.10
26	12	50	12	4	0.5	1.28016	4.320	12.75
8	13	50	12	6	1.0	1.18753	3.165	11.85
2	14	75	6	4	0.5	1.76118	7.245	20.55
18	15	75	12	2	0.5	0.75572	4.980	14.90
22	16	50	18	4	0.0	0.87371	4.545	14.60
21	17	50	6	4	0.0	0.84745	7.755	22.15
7	18	50	12	2	1.0	0.79661	2.745	11.55
19	19	25	12	6	0.5	1.15705	3.330	12.45
3	20	25	18	4	0.5	0.74206	2.625	9.85
4	21	75	18	4	0.5	0.88552	4.350	14.05
14	22	50	18	2	0.5	0.53341	3.075	11.80
1	23	25	6	4	0.5	1.17691	4.080	14.40
25	24	50	12	4	0.5	1.43943	4.410	14.25
11	25	25	12	4	1.0	1.15367	1.965	10.55
6	26	50	12	6	0.0	0.75567	6.315	19.90
12	27	75	12	4	1.0	1.55606	3.600	12.00

current, MWCNT amount) and square model terms with interaction terms of current \times current had contributing roles in deciding the response. This depicts the significance of

these terms. The highest f -value of 17.12 for current shows that it had the highest contributor to affect MRR. The other remaining interaction terms were non-significant, owing to

Fig. 2 Machined specimens as per L27 design of BBD

Table 4 ANOVA for MRR

Source	DoF	SS	MS	F	P	Significance
Model	7	2.33107	0.333011	8.28	0.000	*
Linear	4	1.98762	0.496905	12.35	0.000	*
T_{on}	1	0.27156	0.271564	6.75	0.018	*
T_{off}	1	0.60312	0.603122	14.99	0.001	*
Current	1	0.71273	0.712729	17.72	0.000	*
MWCNT	1	0.40021	0.400207	9.95	0.005	*
Square	2	0.24390	0.121950	3.03	0.007	*
Current × current	1	0.17218	0.172175	4.28	0.002	*
MWCNT × MWCNT	1	0.11930	0.119296	2.97	0.101	**
2-way interaction	1	0.09955	0.099552	2.47	0.132	**
Current × MWCNT	1	0.09955	0.099552	2.47	0.132	**
Error	19	0.76432	0.040227			
Lack-of-fit	17	0.75131	0.044195	6.80	0.136	**
Pure error	2	0.01300	0.006501			
Total	26	3.09539				

*Significant term; ** non-significant term

their larger p -values. The value of lack-of-fit was recorded as 0.136, which is more than 0.05, which shows that it is non-significant. This suggested the acceptance of the model. R^2 values near unity were used to evaluate the competence of the developed regressions. R^2 and adj. R^2 , with values of 94.21% and 87.71%, respectively, has shown the acceptability of the model with the least variation.

ANOVA for SR was depicted in Table 5. The entire model term, linear model term, square interactions, and 2-way interactions illustrated that all these models and interactions significantly impacted deciding SR response. Entire linear model variables, such as T_{on} , T_{off} , current, and MWCNT amount, were found to have a big effect on SR response. The maximum f -value of 2352.39 indicates

Table 5 ANOVA for SR

Source	DoF	SS	MS	F	P	Significance
Model	12	61.9848	5.1654	480.78	0.000	*
Linear	4	59.2309	14.8077	1378.26	0.000	*
T_{on}	1	17.1363	17.1363	1595.00	0.000	*
T_{off}	1	15.2551	15.2551	1419.90	0.000	*
Current	1	1.5660	1.5660	145.76	0.000	*
MWCNT	1	25.2735	25.2735	2352.39	0.000	*
Square	2	0.5871	0.2935	27.32	0.000	*
$T_{on} \times T_{on}$	1	0.0456	0.0456	4.24	0.050	*
$T_{off} \times T_{off}$	1	0.4601	0.4601	42.83	0.000	*
2-way interaction	6	2.1669	0.3611	33.61	0.000	*
$T_{on} \times T_{off}$	1	0.5184	0.5184	48.25	0.000	*
$T_{on} \times \text{current}$	1	0.0812	0.0812	7.56	0.016	*
$T_{on} \times \text{MWCNT}$	1	0.6320	0.6320	58.83	0.000	*
$T_{off} \times \text{current}$	1	0.0541	0.0541	5.03	0.042	*
$T_{off} \times \text{MWCNT}$	1	0.8236	0.8236	76.65	0.000	*
Current × MWCNT	1	0.0576	0.0576	5.36	0.036	*
Error	14	0.1504	0.0107			
Lack-of-fit	12	0.1390	0.0116	2.03	0.377	**
Pure error	2	0.0114	0.0057			
Total	26	62.1352				

*Significant term; ** non-significant term

that the MWCNT amount has a large contributor, followed by T_{off} . Square interaction including $T_{\text{on}} \times T_{\text{on}}$, $T_{\text{off}} \times T_{\text{off}}$ terms and 2-way interaction model including of $T_{\text{on}} \times T_{\text{off}}$, $T_{\text{on}} \times \text{current}$, $T_{\text{on}} \times \text{MWCNT}$, $T_{\text{off}} \times \text{current}$, $T_{\text{off}} \times \text{MWCNT}$ were having a substantial effect. The other remaining interaction terms were observed to be non-significant owing to their larger p -values. The value of lack-of-fit was recorded as 0.377, which is more than 0.05, which shows that it is non-significant. This suggested the acceptance of the model. R^2 values near unity were used to evaluate the competence of the developed regressions. R^2 and adj. R^2 , with values of 99.76% and 99.55%, respectively, has shown the model's acceptability with the least variation.

A statistical analysis of RLT was represented in Table 6 by using the ANOVA technique. The entire model term, linear model term, square interactions, and 2-way interactions were represented that all these models and interactions had a significant effect on determining RLT. All variables of the linear model term, such as T_{on} , T_{off} , current, and MWCNT amount, had a big effect on determining RLT values. The maximum f -value of 482.95 indicates that the MWCNT amount has a

large contributor, followed by T_{off} . Square interaction including $T_{\text{off}} \times T_{\text{off}}$, current \times current terms and 2-way interaction model including $T_{\text{on}} \times \text{current}$, $T_{\text{on}} \times \text{MWCNT}$, $T_{\text{off}} \times \text{current}$, $T_{\text{off}} \times \text{MWCNT}$, current \times MWCNT were having a substantial effect. The other remaining interaction terms were observed to be non-significant owing to their more significant p -value of 0.05. The value of lack-of-fit was recorded as 0.949, which is far larger than 0.05, showing that it is non-significant. This suggested the acceptance of the model. R^2 values near unity were used to evaluate the competence of the developed regressions. R^2 and adj. R^2 , with values of 99.04% and 98.07%, respectively, has shown the model's acceptability with the least variation [49].

3.3 Regression equations

To understand the relationship between the WEDM parameters and responses, mathematical correlations were generated through BBD design for all responses by using Minitab v17. Equations (2), (3) and (4) depict the regressions for responses of MRR, SR, and RLT, respectively.

$$\begin{aligned} \text{MRR} = & 0.2290 + 0.0060 \cdot T_{\text{on}} - 0.0374 \cdot T_{\text{off}} + 0.3710 \cdot \text{current} + 0.2800 \cdot \text{MWCNT} \\ & - 0.0410 \cdot \text{current} \cdot \text{current} - 0.5460 \cdot \text{MWCNT} \cdot \text{MWCNT} + 0.1800 \cdot \text{current} \cdot \text{MWCNT} \end{aligned} \quad (2)$$

Table 6 ANOVA for RLT

Source	DoF	SS	MS	F	P	Significance
Model	13	317.347	24.411	102.78	0.000	*
Linear	4	286.279	71.570	301.35	0.000	*
T_{on}	1	70.810	70.810	298.15	0.000	*
T_{off}	1	81.641	81.641	343.75	0.000	*
Current	1	19.127	19.127	80.53	0.000	*
MWCNT	1	114.701	114.701	482.95	0.000	*
Square	3	6.247	2.082	8.77	0.002	*
$T_{\text{off}} \times T_{\text{off}}$	1	4.660	4.660	19.62	0.001	*
Current \times current	1	3.046	3.046	12.82	0.003	*
MWCNT \times MWCNT	1	0.930	0.930	3.92	0.069	**
2-way interaction	6	24.821	4.137	17.42	0.000	*
$T_{\text{on}} \times T_{\text{off}}$	1	0.951	0.951	4.00	0.067	**
$T_{\text{on}} \times \text{current}$	1	3.802	3.802	16.01	0.002	*
$T_{\text{on}} \times \text{MWCNT}$	1	10.562	10.562	44.47	0.000	*
$T_{\text{off}} \times \text{current}$	1	1.381	1.381	5.81	0.031	*
$T_{\text{off}} \times \text{MWCNT}$	1	5.062	5.062	21.32	0.000	*
Current \times MWCNT	1	3.063	3.063	12.89	0.003	*
Error	13	3.088	0.238			
Lack-of-fit	11	1.796	0.163	0.25	0.949	**
Pure error	2	1.292	0.646			
Total	26	320.435				

*Significant term; ** non-significant term

Table 7 Results of single-response optimization

Case studies	Input variables				Output parameters		
	T_{on}	T_{off}	Current	MWCNT	MRR	SR	RLT
Max. MRR	75	6	6	1	1.8883	5.41	17.40
Min. SR	25	14	2	1	0.4844	1.89	11.54
Min. RLT	25	16	5	1	1.1357	1.93	9.70

$$\begin{aligned}
 SR = & 4.2210 + 0.0946 \cdot T_{on} - 0.2835 \cdot T_{off} + 0.2144 \cdot \text{current} - 2.6470 \cdot \text{MWCNT} - 0.0001 \cdot T_{on} \cdot T_{on} \\
 & + 0.0075 \cdot T_{off} \cdot T_{off} - 0.0024 \cdot T_{on} \cdot T_{off} + 0.0029 \cdot T_{on} \cdot \text{Current} - 0.0318 \cdot T_{on} \cdot \text{MWCNT} \\
 & - 0.0097 \cdot T_{off} \cdot \text{current} + 0.1512 \cdot T_{off} \cdot \text{MWCNT} - 0.1200 \cdot \text{current} \cdot \text{MWCNT}
 \end{aligned} \tag{3}$$

$$\begin{aligned}
 RLT = & 18.3300 + 0.1232 \cdot T_{on} - 0.8510 \cdot T_{off} - 0.7440 \cdot \text{current} - 2.2600 \cdot \text{MWCNT} + 0.0245 \cdot T_{off} \cdot T_{off} \\
 & + 0.1781 \cdot \text{current} \cdot \text{current} + 1.5750 \cdot \text{MWCNT} \cdot \text{MWCNT} - 0.0033 \cdot T_{on} \cdot T_{off} + 0.0195 \cdot T_{on} \cdot \text{current} \\
 & - 0.1300 \cdot T_{on} \cdot \text{MWCNT} - 0.0490 \cdot T_{off} \cdot \text{current} + 0.3750 \cdot T_{off} \cdot \text{MWCNT} - 0.8750 \cdot \text{current} \cdot \text{MWCNT}
 \end{aligned} \tag{4}$$

3.4 Normal probability plots

Normal probability plots for responses MRR, SR, and RLT are shown in Fig. 3. Verification of these plots yields the validation of ANOVA results for the respective response. For MRR, SR, and RCL, the normal probability shows the plot between the percentages versus the residual. Normality plot verifies that entire the residuals are on a straight line. This shows that the model assumptions are correct and normally distributed errors [50]. Figure 3 shows that all these results were obtained for responses of MRR, SR, and RLT. This verifies the ANOVA results for a better future outcome for proposed models.

3.5 Effect of machining variables on the response

The effect of individual parameters (T_{on} , T_{off} , current, MWCNT amount) was investigated on MRR, SR, and RLT using main effect graphs. The response major effect plots emphasize the best factor-level combinations for a specific response.

3.5.1 Effect of T_{on} on responses

The impact of T_{on} on all the selected response variables was investigated and shown in Fig. 4. As per the ANOVA analysis, T_{on} was found to be an important contributing factor for MRR, SR, and RLT, having a contribution of 13.66%, 28.93%, and 24.73%, respectively. As evident from Fig. 4,

the values of MRR, SR, and RLT increase by rise in T_{on} . Increment of T_{on} from 25 to 75 μs resulted in enhancement of MRR from 0.9250 to 1.2258 g/min. This shows an improvement in MRR of 32.52% with an increased T_{on} from 25 to 75 μs . This was a due rise in discharge energy per spark with the rise in T_{on} [51]. Discharge energy is transformed into thermal energy during WEDM operation. The substance is subsequently melted and vaporized as a result of the thermal energy [52]. Due to this, the rise in T_{on} value enhances the discharge energy, which in turn improves the MRR value. This suggests the desired T_{on} value of 75 μs for attaining enhancement of MRR.

Figure 4 shows a continuous increment in SR value with the rise in T_{on} . SR was increased from 3.16 to 5.55 μm , with the increased value of T_{on} from 25 to 75 μs . This shows a negative effect of increased T_{on} on SR response of 75.63% effect. A rise in T_{on} also raises discharge energy, which raises thermal energy. SR of the machined product is severely influenced by the size of the craters generated during the machining operation when the material gets eroded [53]. The primary cause of debris creation is thermal energy generated by discharge energy. Increased thermal energy causes wider and deeper craters on machined surfaces along with the deterioration of the workpiece [54]. This suggests the desired T_{on} value of 25 μs for attaining the least value of RLT.

A similar trend like SR value was also depicted for RLT with the rise in T_{on} . A negative effect of increased T_{on} was found for RLT, which shows a rise in RLT value from 12.07 to 16.93 μm , having a negative impact of 40.26%. An increase in the T_{on} also increases discharge energy per

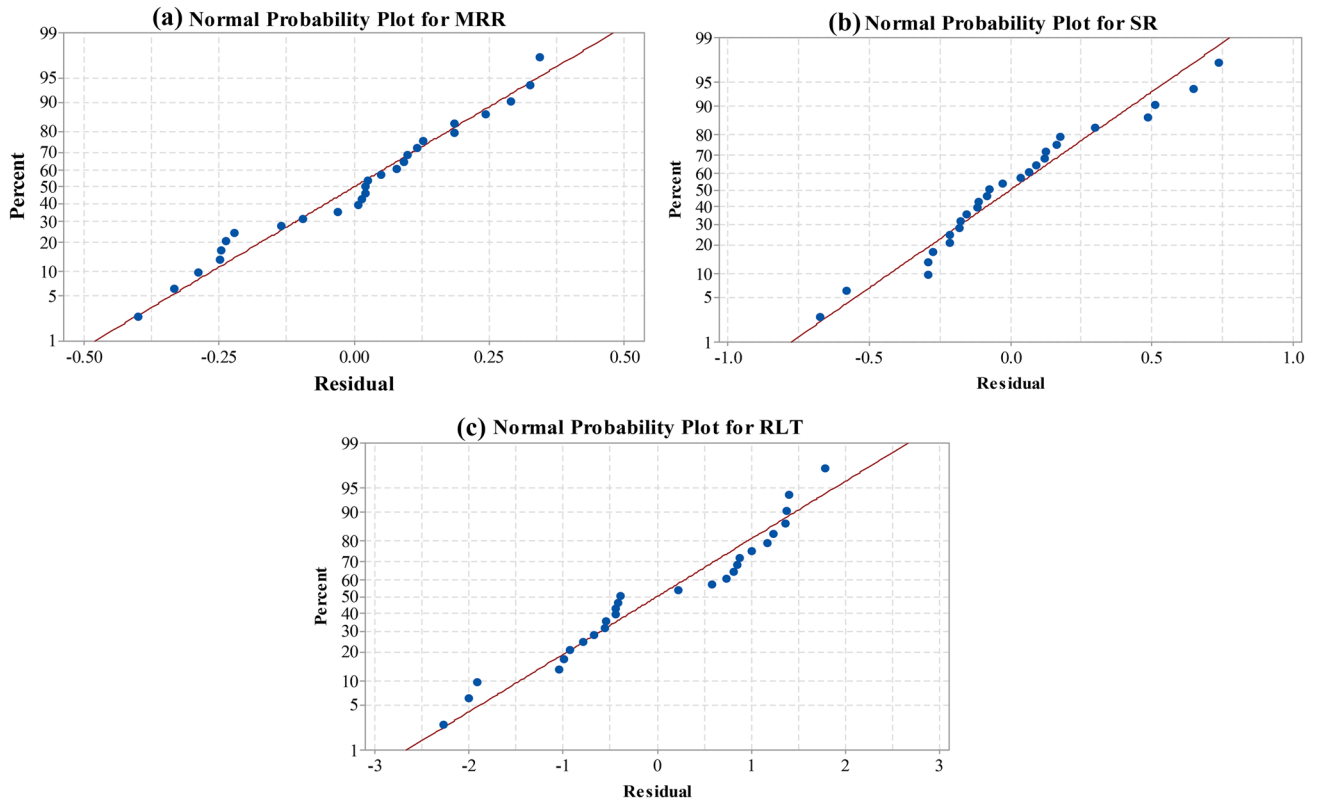


Fig. 3 Normal probability plot for a MRR, b SR, and c RLT

spark. A substantial amount of heat gets transmitted in the machining area due to the current rise [55]. Due to this heat, the amount of molten metal grows. The accumulated debris particles then get deposited on work material [56]. These molten metals are then quenched and re-solidified, forming a thick layer on work material known as RLT. This suggests the desired T_{on} value of 25 μs for attaining the least value of RLT.

3.5.2 Effect of T_{off} on responses

The impact of T_{off} on all response variables is shown in Fig. 5. X- and Y-axes of Fig. 5 represent the T_{off} and responses, respectively. ANOVA analysis has shown that T_{off} had a substantial influence on determining MRR, SR, and RLT values with a contribution of 30.34%, 25.75%, and 28.51%, respectively.

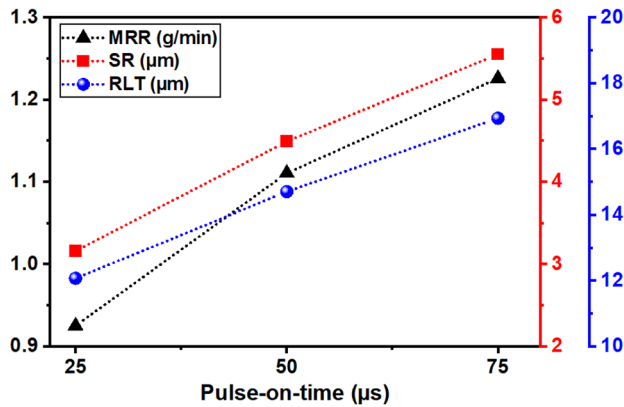


Fig. 4 Significance of T_{on} on responses

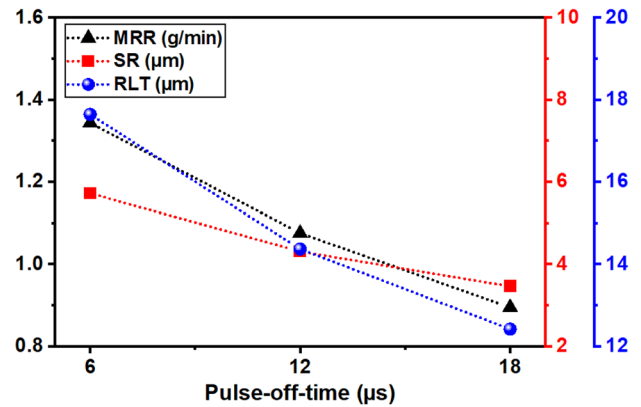


Fig. 5 Significance of T_{off} on responses

Figure 5 shows a declined trend for all responses with an increased value of T_{off} . MRR had decreased to 0.8948 g/min from 1.3432 g/min when T_{off} increased from 6 to 18 μ s. This shows a decline of 33.38% in MRR with the increased value of T_{off} . The graph depicts the inverse effect of increasing T_{off} on MRR. An increase in T_{off} enlarges the interval between two consecutive sparks, reducing the number of active sparks [57]. Lower discharge energy will be achieved with larger T_{off} values. As a result of this, as T_{off} propagates, MRR decreases owing to a drop in spark, lowering the discharge energy.

Figure 5 shows a continuous decrement in SR value with the rise in T_{off} . SR was reduced to 3.46 from 5.72 μ m with an increased value of T_{off} from 6 to 18 μ s. This shows an SR of 39.51% improvement with an increased T_{off} from 6 to 18 μ s. The graph depicts a drop in SR with a rise in T_{off} due to the formation of tiny craters. Increased value of T_{off} reduces active sparks, which results in lower thermal energy [58]. This, in turn, forms tiny craters on the workpiece and improves surface quality by reducing the SR.

A similar declined trend for RLT was illustrated in Fig. 5 with an increased value of T_{off} . RLT reduced from 17.64 to 12.42 μ m with an increased value of T_{off} from 6 to 18 μ s. This shows an improvement in RLT of 29.59% with an increased T_{off} from 6 to 18 μ s. This is due to a reduction in material melting, and lower T_{off} allows the eroded particles to flush away. This is due to a reduction in the melting of material, and lower T_{off} allows the eroded particles to flush away from the gap of the work-tool interface [59].

3.5.3 Effect of current on responses

The impact of current on all the selected response variables was investigated and shown in Fig. 6. As per the ANOVA analysis, the current was found to be an important contributing factor for MRR, SR, and RLT, having a contribution of 35.85%, 2.64%, and 6.68%, respectively. As evident from Fig. 6, the values of MRR, SR, and RLT increase by the rise in current. Increment in

current from 2 to 6 A resulted in an enhancement of MRR from 0.7752 to 1.2626 g/min. This shows an improvement in MRR of 62.87% with an increased current from 2 to 6 A. This was due to increased discharge energy per spark. Discharge energy is transformed into thermal energy during WEDM performance [60]. The substance is subsequently melted and vaporized as a result of the thermal energy. A rise in current, on the other hand, raises discharge energy, which raises the MRR value [61]. This suggests the desired current value of 6A for attaining enhancement of MRR.

A drop in SR was observed with the enhancement of current from 2 to 6 A, as per Fig. 6. SR was increased to 4.77 from 4.05 μ m with an increased value of current from 2 to 6 A. This shows a negative effect of increased current on SR response of 17.77% effect. The discharge energy of the process increases, which in turn escalates the thermal energy of the sparks. Ionization of distilled water occurs at larger values of current due to high discharge and thermal energy, the formation of bigger and deeper craters, and an increase in SR [62]. This suggests the desired current value of 2A for attaining the least value of SR.

A declined trend was also depicted for RLT with a rise in current. A negative effect of increased current was found for RLT, which shows a rise in RLT value from 13.65 to 16.18 μ m, having a negative impact of 18.53%. An increase in the current increases discharges energy per spark. A substantial amount of heat gets transmitted in the machining area due to the current rise [55]. Due to this heat, the amount of molten metal grows. The accumulated debris particles then get deposited on work material [23]. These molten metals are then quenched and re-solidified and form a thick RLT. This suggests the desired current value of 2A for attaining the least value of RLT.

3.5.4 Effect of MWCNT on responses

The importance of MWCNT amount on all response variables is shown in Fig. 6. X- and Y-axes of Fig. 7 represent

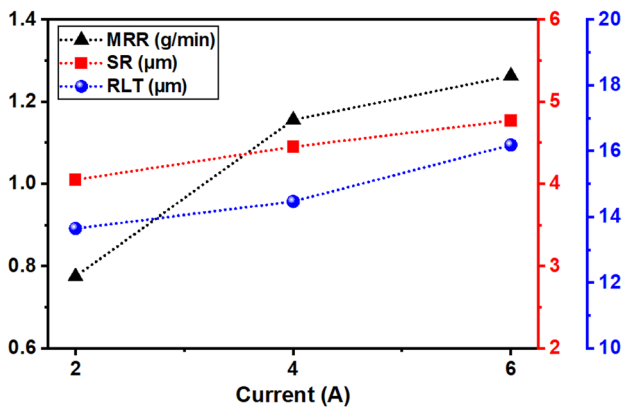


Fig. 6 Significance of current responses

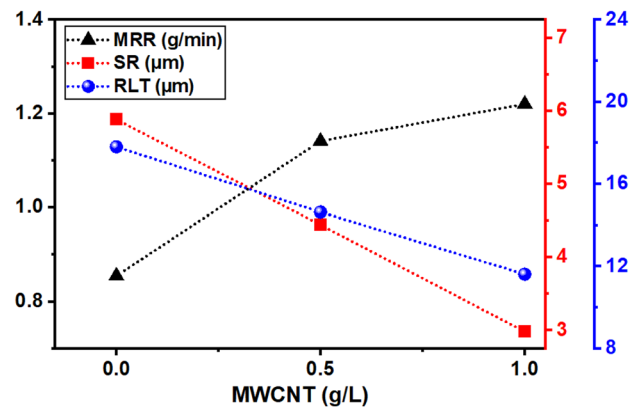


Fig. 7 Significance of MWCNT on responses

the MWCNT amount and responses, respectively. ANOVA analysis has demonstrated that MWCNT substantially influences the MRR, SR, and RLT values with 20.13%, 42.66%, and 40.07%, respectively. Figure 7 shows a substantial improvement for all responses with the increased value of the MWCNT amount. MRR value has been observed to be improved with the addition of MWCNT amount to 1 g/L. A 42.73% of improvement was measured for MRR with a rise in mean value from 0.8546 to 1.2198 g/min. An increase in MWCNT amount permits larger ions to transfer from work material owing to improved conductivity of MWCNT amount in IEG [63]. MWCNT amount enriches thermal conductivity and sparking distribution. This causes an escalation in MRR value with intensifications in the erosion rate. Obtained results have shown that MWCNT with 1 g/L largely enhanced MRR value.

Figure 7 also shows a positive effect of MWCNT amount on SR as it decreases from 5.88 to 2.98 μm with the addition of MWCNT amount to 1 g/L. This means a 49.32% of improvement was found for SR. Addition of MWCNT amount expands the inter-electrode gap by reducing the insulation strength of the dielectric. This creates a small crater

on machined components and improves the surface quality. Debris get flushed away easily from the machining zone with the addition of MWCNT. Small ridges are then formed owing to this enhanced flushing of debris, thereby improving the surface quality [63]. Due to this, the SR reduces with the rise of the MWCNT amount. Obtained results have shown that MWCNT with 1 g/L substantially reduced SR value.

A similar observation was found for RLT, where an increase in MWCNT amount was again having a constructive outcome on RLT. RLT declined from 17.80 to 11.61 μm with an increased value of MWCNT amount from 0 to 1 g/L. This shows an improvement in RLT of 34.77% with an increased MWCNT amount. As the MWCNT amount enlarges, the inter-electrode gap, along with an increase in heat dissipation in the dielectric fluid, generates small craters and reduces plasma heat flux [29]. Debris get flushed away easily from the machining zone with the addition of MWCNT. The addition of MWCNTs decreases the insulation strength of the dielectric, and this further raises the inter-electrode gap, thereby lowering the RLT [64]. Obtained results have shown that MWCNT with 1 g/L substantially reduced RLT.

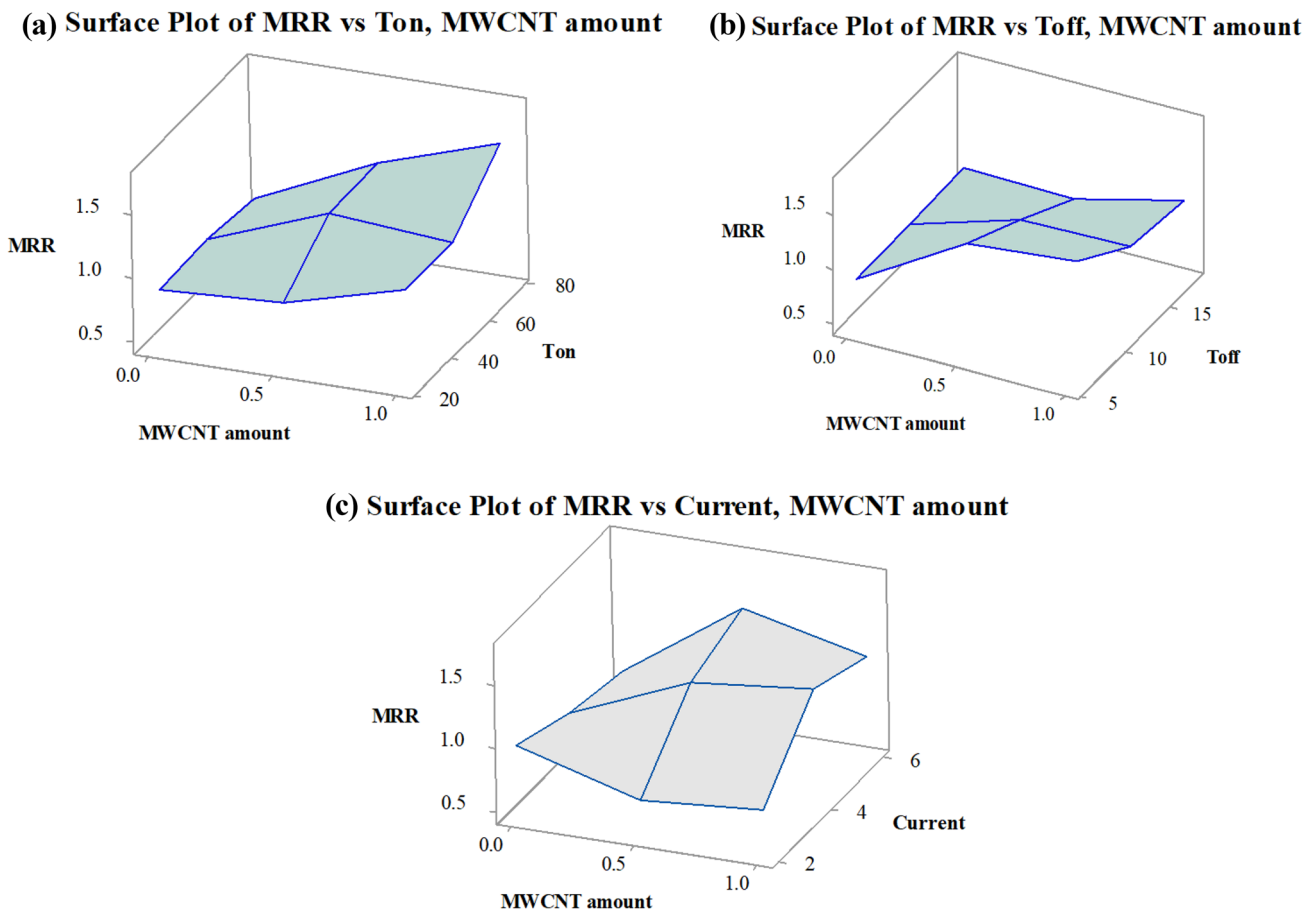


Fig. 8 3D surface plots for MRR

3.6 Combined effect process parameters on responses using 3D surface plots

3.6.1 3D surface plots for MRR

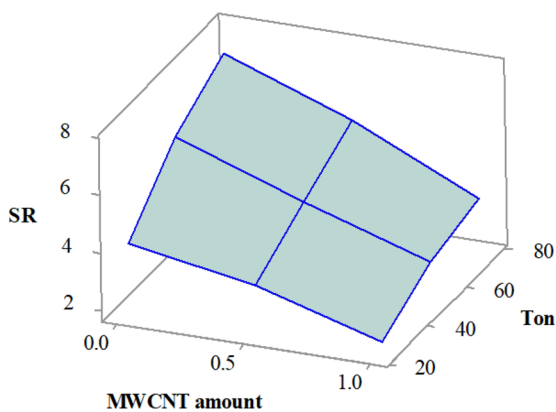
3D surface plots for MRR were used to demonstrate the effect of two process variables by keeping the other input variables at a constant level. Figure 8a–c shows a 3D surface plot for MRR. As discussed in the previous section of the main effect plot, the addition of the MWCNT amount was found to have a positive effect on all the responses. Therefore, the effect of MWCNT, along with other remaining responses, was studied by using 3D surface plots. Figure 8a represents the plot of MRR vs. T_{on} , and MWCNT amount, wherein an ascending tendency of MRR was demonstrated with a rise in the values of both T_{on} and MWCNT amount. The maximum value of MRR was calculated at T_{on} of 75 μ s, and MWCNT amount of 1 g/L, while minimum MRR was obtained at T_{on} of 25 μ s, and MWCNT amount of 0 g/L. This suggests that both T_{on} and MWCNT amounts were found to have a positive effect on

the improvement of MRR. In Fig. 8b, MRR intensified with the rise of MWCNT and declined with the rise of T_{off} . Corresponding values for maximum MRR of T_{off} and MWCNT amount were 1 g/L and 6 μ s, respectively, while least MRR was obtained at 0 g/L and 6 μ s of T_{off} and MWCNT amount, respectively. The same level of T_{off} for maximum and minimum MRR shows that it did not have a large impact on deciding MRR compared to the MWCNT amount. From Fig. 8c, the largest value of MRR was noticed at 6 A of current and 0.5 g/L MWCNT amount, while the smallest value of MRR was observed at 2 A of current and 0 g/L MWCNT amount. This clearly suggested that current has shown a significant influence on the enhancement of MRR. This was also evident from ANOVA analysis.

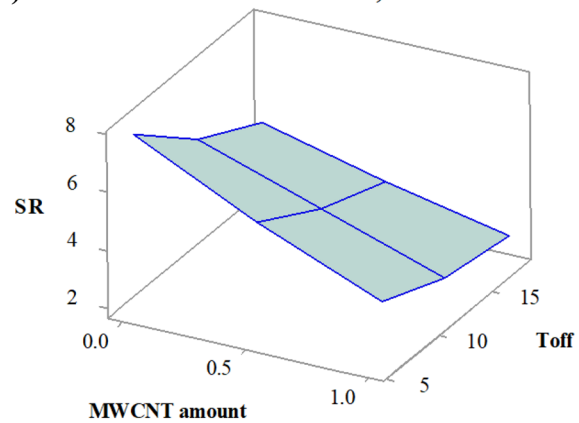
3.6.2 3D surface plots for SR

3D surface graphs for SR were plotted as per Fig. 9a–c, and it was analyzed by changing two parameters and retaining the remaining variables at a constant level. From Fig. 9a,

(a) Surface Plot of SR vs T_{on} , MWCNT amount



(b) Surface Plot of SR vs T_{off} , MWCNT amount



(c) Surface Plot of SR vs Current, MWCNT amount

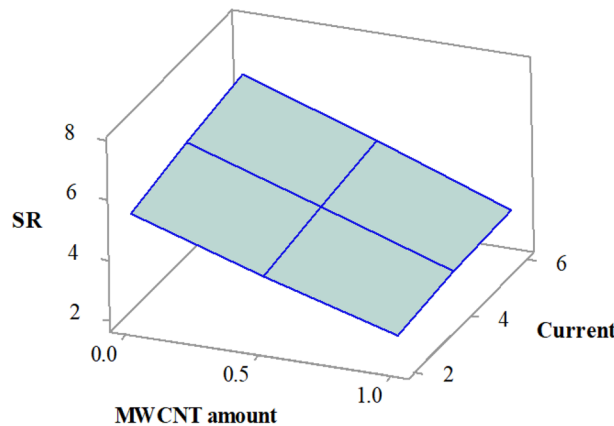


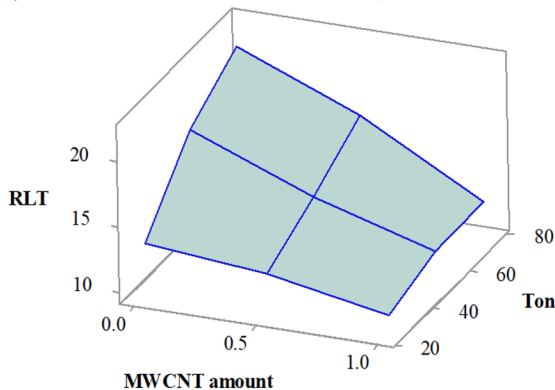
Fig. 9 3D surface plots for SR

a continuous downtrend was detected with an increase in MWCNT amount and a drop in T_{on} . The lowest SR value was measured at T_{on} of 25 μ s and MWCNT amount of 1 g/L. The exact opposite trend was noticed for maximum SR, which shows the corresponding levels of 75 μ s and 1 g/L for T_{on} and MWCNT amount, respectively. This clearly shows that an increased MWCNT amount improves the surface quality. In Fig. 9b, a continuous downtrend for SR was depicted with increased values of both T_{off} and MWCNT amount. The maximum value of SR was calculated at T_{off} of 6 μ s and MWCNT amount of 0 g/L, while the least SR was obtained at T_{off} of 18 μ s and MWCNT amount of 1 g/L. This was also evident from ANOVA analysis and main effect plots. Figure 9c shows the graph for SR vs. the current MWCNT amount. SR was found to be minimum at the lowest level current and the highest level of MWCNT amount. The linear trend of rising and drop of SR was found, which gives the least value at the current of 2 A and MWCNT amount of 1 g/L, while the largest SR at the current of 6 A and MWCNT amount of 0 g/L. This clearly shows the importance of MWCNT addition in dielectric fluid.

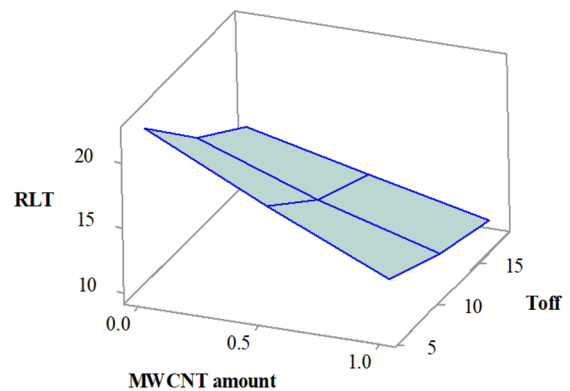
3.6.3 3D surface plots for RLT

Figure 10a–c shows the 3D surface plot for RLT by changing two parameters and retaining the remaining variables at a constant level. From Fig. 10a, a continuous downtrend was detected with an increase in MWCNT amount and a drop in T_{on} . The lowest RLT value was measured at T_{on} of 25 μ s and MWCNT amount of 1 g/L. An exactly opposite trend was noticed for maximum RLT, which shows the corresponding levels of 75 μ s and 1 g/L for T_{on} and MWCNT amount, respectively. This clearly shows that an increased MWCNT amount improves the surface quality. In Fig. 10b, a continuous downtrend for RLT was depicted with increased values of both T_{off} and MWCNT amount. The maximum value of RLT was calculated at T_{off} of 6 μ s and MWCNT amount of 0 g/L, while the least RLT was obtained at T_{off} of 18 μ s and MWCNT amount of 1 g/L. This was also evident from ANOVA analysis and main effect plots. Figure 10c shows the graph for RLT vs. the current MWCNT amount. RLT was found to be minimum at the lowest level current and the highest level of MWCNT amount. The linear trend of rising and drop of RLT was found, which gives the least

(a) Surface Plot of RLT vs Ton, MWCNT amount



(b) Surface Plot of RLT vs Toff, MWCNT amount



(c) Surface Plot of RLT vs Current, MWCNT amount

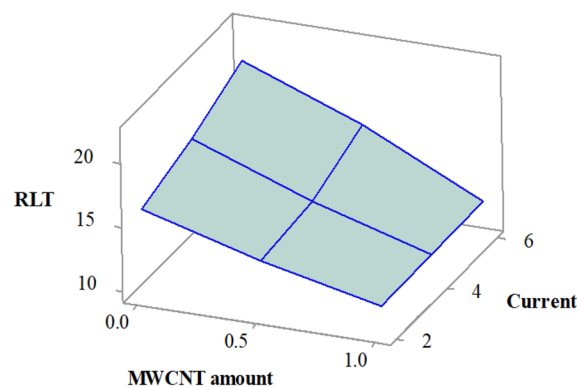


Fig. 10 3D surface plots for RLT

value at the current of 2 A and MWCNT amount of 1 g/L, while the largest RLT at the current of 6A and MWCNT amount of 0 g/L.

3.7 Optimization using PVS algorithm

ANOVA analysis, main effect plots, and 3D surface plots have shown that MRR, SR, and RLT responses had different levels of input process parameters. To accomplish all the objectives, the passing vehicle search (PVS) algorithm was employed. PVS algorithm was observed to have easy during implementation. During the algorithm's execution, MRR was considered as the maximum, while SR and RLT were considered as a minimum. The condition of response variables (MRR, SR, and RLT) was considered as positive numerals through the execution of PVS optimization. Upper and lower bound levels of WEDM variables were considered for the implementation of the PVS algorithm. Thus, levels of WEDM parameters with T_{on} from 25 to 50 μ s; T_{off} from 6 to 18 μ s; current from 2 to 6 A; and MWCNT amount from 0 to 1 g/L were selected for optimization. Different case studies were considered during the execution of the algorithm. Case studies pertaining to this optimization include single-objective optimization and simultaneous optimization of responses. Table 7 shows the obtained results of single-response optimization. Case A: Maximum MRR.

3.7.1 Case A: Maximum MRR

A larger erosion rate is preferable as it enhances productivity and makes the manufacturing process cost-effective. Therefore, the objective function of maximum MRR was considered as per Eq. (5):

$$\text{Obj}(v_1) = \max.(\text{MRR}) \quad (5)$$

Maximization MRR objective function yielded the highest possible value of 1.8883 g/min. The corresponding WEDM variables at this maximum MRR were found as T_{on} with 75 μ s, T_{off} with 6 μ s, current with 6 A, and MWCNT with 1 g/L. A confirmatory trial was conducted for verification of attained outcomes. The experimentally attained value of MRR was witnessed as 1.9112 g/min, which shows a minor error of 1.19%. It clearly reveals the acceptance of the PVS technique.

3.7.2 Case B: Minimum SR

The quality of the machined components was largely assessed by the SR parameter. This means the least value of SR desirable for obtaining better quality machined components. Therefore, the objective function of minimum SR was considered as per Eq. (6):

$$\text{Obj}(v_2) = \min.(\text{SR}) \quad (6)$$

The minimization of the SR objective function yielded the lowest possible value of 1.89 μ m. The corresponding input parameters of T_{on} with 25 μ s, T_{off} with 14 μ s, current with 2 A, and MWCNT amount with 1 g/L were obtained for the least SR value. The experimentally attained value of SR was witnessed to be 1.93 μ m which shows a minor error of 2.07%. This suggests the adequacy and fitness of the PVS algorithm.

3.7.3 Case C: Minimization of RLT

RLT represents a thickness for the deposition and solidification of molten material which gets formed during the process. Therefore, to acquire great surface quality with minimal surface irregularities, the smallest RLT is anticipated. Therefore, the objective function of minimum SR was considered as per Eq. (7):

$$\text{Obj}(v_3) = \min.(\text{RLT}) \quad (7)$$

The minimization of the RLT objective function yielded the lowest possible value of 9.7 μ m. The corresponding input parameters of T_{on} with 25 μ s, T_{off} with 16 μ s, current with 5 A, and MWCNT amount with 1 g/L were obtained for the least RLT value. The experimentally attained value of SR was witnessed to be 9.86 μ m which shows a minor error of 2.1%.

3.7.4 Case D: Simultaneous optimization of all responses

By considering the importance of all the process variables, simultaneous optimization was carried out by assigning equal weights to all responses. Therefore, the objective function as per Eq. (8) is developed for all responses.

$$\text{Obj}(v_4) = w_1 \cdot (\text{MRR}) + w_2 \cdot (\text{SR}) + w_3 \cdot (\text{RLT}) \quad (8)$$

The above objective function yielded results of MRR with 1.3318 g/min, SR with 2.09 μ m, RLT with 10.24 μ m values at WEDM variables of T_{on} with 26 μ s, T_{off} with 13 μ s, current with 6 A, and MWCNT with 1 g/L. Validation of these predicted values from the PVS algorithm was carried out by conducting the experiment at obtained input parameters. Responses were then measured, showing the MRR with 1.3772 g/min, SR with 2.14 μ m, and RLT with 10.09 μ m values. Results of actual trials specified an acceptable error of 3.29%, 2.33%, and 1.48% for MRR, SR, and RLT, respectively. It clearly reveals the acceptance of the PVS technique in the present study for Udimet 720.

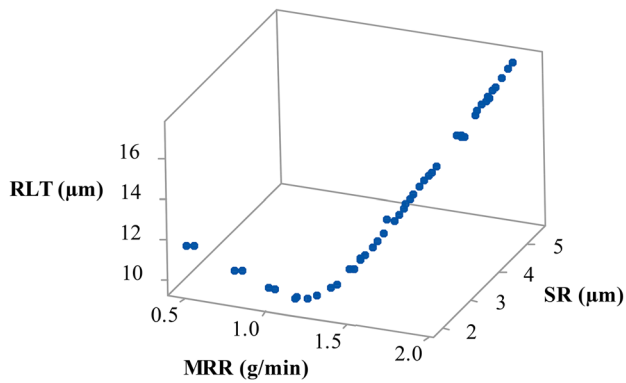


Fig. 11 Pareto plot of MRR vs. SR vs. RLT

Apart from simultaneous optimization, a set of non-dominated solutions were obtained through Pareto optimal fronts. For MRR maximization, the SR and RLT values were $5.41 \mu\text{m}$ and $17.40 \mu\text{m}$, which are far from their required levels. Such a scenario may be effectively tackled by Pareto's optimal points. In essence, Pareto fronts provide a trade-off between two competing objectives, and producers can choose any point on the front. Figure 11 displays the Pareto graph. The contradictory nature of the graph is clear, as an increment in MRR has a negative effect on SR and RLT. Users will have an option to select the suitable Pareto point by considering their requirement of response values. Random experiments were conducted from Pareto points to verify the adequacy of projected results. A small acceptable deviation was detected among the actual and forecasted results from PVS algorithm. It clearly reveals the acceptance of PVS technique in the present study for Udimet 720.

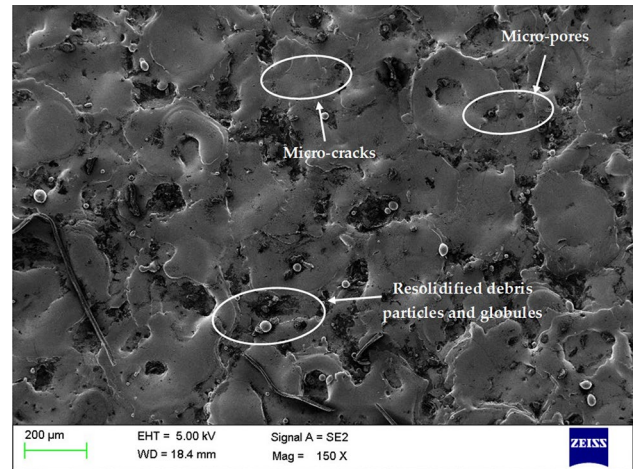


Fig. 13 SEM image at T_{on} with $26 \mu\text{s}$, T_{off} with $13 \mu\text{s}$, current with 6 A, and MWCNT amount with 0.5 g/L values

3.8 Impact of MWCNT on surface morphology

ANOVA analysis, main effect plots, and 3D surface plots were shown to have a large significance of MWCNT amount on responses. MWCNT was also having large contributor to the reduction in SR and RLT responses. Thus, it becomes vital to comprehend the behavior of MWCNT amount on surface textures of machined components. Pursuant to this, optimized parameters of case study IV were considered as this objective function gives the optimal solution by considering the equal importance of all the responses. Optimized parameters include T_{on} with $26 \mu\text{s}$, T_{off} with $13 \mu\text{s}$, and current with 6 A, wherein MWCNT amount was varied from 0 to 1 g/L to understand its effect. Figures 12, 13 and 14 show

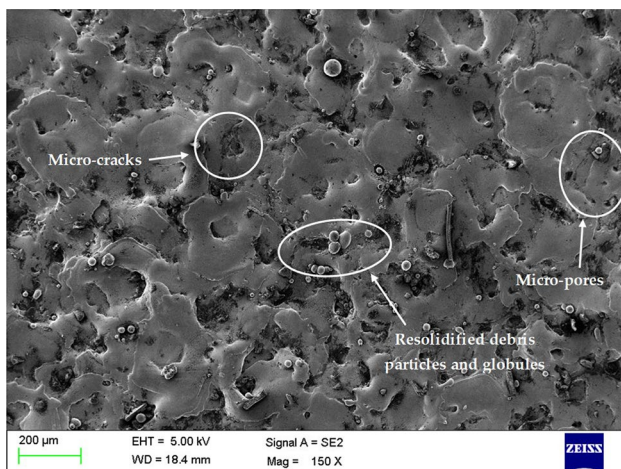


Fig. 12 SEM image at T_{on} with $26 \mu\text{s}$, T_{off} with $13 \mu\text{s}$, current with 6 A, and MWCNT amount with 0 g/L values

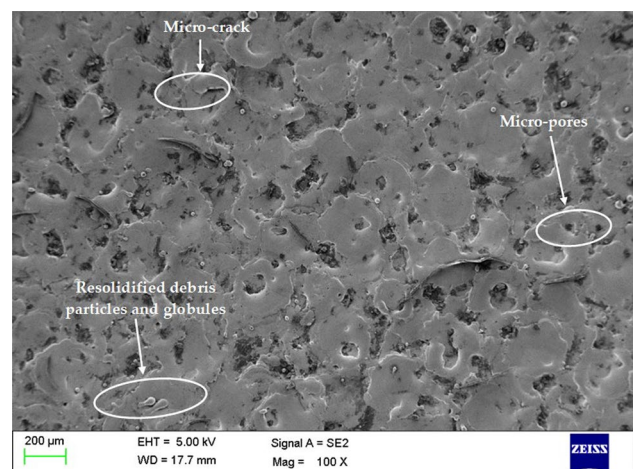


Fig. 14 SEM image at T_{on} with $26 \mu\text{s}$, T_{off} with $13 \mu\text{s}$, current with 6 A, and MWCNT amount with 1 g/L values

the SEM of machined Udimet 720 at MWCNT amounts of 0 g/L, 0.5 g/L, and 1 g/L, respectively. Figure 12 for conventional WEDM (MWCNT amount 0 g/L) reveals a substantial presence of micro-pores, large globules, unflushed debris, and the existence of micro-cracks. Figure 13 for MWCNT amount of 0.5 g/L has shown small improvement in comparison with surface obtained conventional WEDM. On the other hand, machined surface produced as per Fig. 14 obtained at MWCNT of 1 g/L amount has shown a lot more improved surface. As per Fig. 14, negligible surface defects such as the minor presence of micro-pores, micro-cracks, globules, and unflushed debris were detected. The consistent sparking among electrodes and workpieces due to the presence of MWCNT has shown a substantial reduction of micro-cracks [64]. The considerable expansion between tool and workpiece due to the addition of MWCNTs creates small craters, which in turn reduces the deposition of debris (globules) and micro-pores. MWCNTs result in the proper and simple flushing of debris [41, 65]. This simple removal of dirt has produced tiny ridges, which further improved the surface quality. Additionally, the high thermal conductivity of MWCNTs increases the heat dissipation and thereby decreases plasma heat flux [31]. Pertaining to these reasons, a considerable drop in surface defects was achieved. This clearly exhibited that MWCNTs mixed at 1 g/L have substantially enhanced the machined surface of Udimet 720.

4 Conclusion

The current study demonstrated the experimental investigations for WEDM machining of Udimet 720 and the use of MWCNT amount. BBD matrix was utilized to design the experimental matrix by considering T_{on} , T_{off} , current, and MWCNT amount as input parameters and MRR, SR, and RLT as responses. Below mentioned findings were drawn from the current study.

- From ANOVA, regression model term, linear model term, square interactions, and 2-way interactions were depicted as having a significant impact on all responses of MRR, SR, and RLT. This shows the suitability of the model. The current was observed to be the highest contributor with 35.85% contribution to affect MRR, while MWCNT amount was found to be the highest contributor for deciding the values of both SR and RLT with contributions of 42.66% and 40.07%, respectively.
- Mathematical correlations were generated through BBD design for all responses. The normal probability plot has verified the outcome of these developed equations. These plots have confirmed ANOVA results for a better future outcome for proposed models.

- Lack-of-fit was detected as non-significance along with close values of R^2 for all responses, and has shown the adequacy of the developed model.
- PVS algorithm was executed by considering all responses as positive numerals. Case studies on single-response optimization have produced the largest MRR with 1.8883 g/min, least SR with 1.89 μm , and least RLT with 9.70 μm values.
- By considering the importance of all the process variables, simultaneous optimization was carried out by assigning equal weights to all responses. It yielded results of MRR with 1.3318 g/min, SR with 2.09 μm , RLT with 10.24 μm values at WEDM variables of T_{on} with 26 μs , T_{off} with 13 μs , current with 6 A, and MWCNT with 1 g/L.
- Additionally, a set of non-dominated solutions was obtained through Pareto optimal fronts. Pareto fronts provide a trade-off between two competing objectives, and producers can choose any point on the front.
- A small acceptable deviation was detected among the actual and forecasted results from the PVS algorithm. It clearly reveals the acceptance of the PVS technique in the present study for Udimet 720.
- SEM analysis revealed that a considerable drop in surface defects (such as micro-pores, large globules, unflushed debris, and micro-cracks) was achieved by using the MWCNT amount at 1 g/L. Obtained SEM results at 0 g/L, 0.5 g/L, 1 g/L demonstrated that the use of MWCNTs at 1 g/L has significantly improved the machined surface of Udimet 720 to a larger extent.

Author contribution All authors contributed to the study conception and design. Material preparation, data collection, and analysis were performed by Rakesh Chaudhari. The first draft of the manuscript was written by Rakesh Chaudhari and all authors commented on previous versions of the manuscript. All authors read and approved the final manuscript.

Funding Open Access funding provided thanks to the CRUE-CSIC agreement with Springer Nature.

Declarations

Competing interests The authors have no relevant financial or non-financial interests to disclose.

Open Access This article is licensed under a Creative Commons Attribution 4.0 International License, which permits use, sharing, adaptation, distribution and reproduction in any medium or format, as long as you give appropriate credit to the original author(s) and the source, provide a link to the Creative Commons licence, and indicate if changes were made. The images or other third party material in this article are included in the article's Creative Commons licence, unless indicated otherwise in a credit line to the material. If material is not included in the article's Creative Commons licence and your intended use is not permitted by statutory regulation or exceeds the permitted use, you will need to obtain permission directly from the copyright holder. To view a copy of this licence, visit <http://creativecommons.org/licenses/by/4.0/>.

References

- Nain SS, Garg D, Kumar S (2018) Investigation for obtaining the optimal solution for improving the performance of WEDM of super alloy Udimet-L605 using particle swarm optimization. *Eng Sci Technol Int J* 21(2):261–273
- Korkmaz ME, Yaşar N, Günay M (2020) Numerical and experimental investigation of cutting forces in turning of Nimonic 80A superalloy. *Eng Sci Technol Int J* 23(3):664–673
- Zhang C et al (2020) Surface integrity of holes machined by electrochemical discharge drilling method. *CIRP J Manuf Sci Technol* 31:643–651
- Vora J et al (2022) Machining parameter optimization and experimental investigations of nano-graphene mixed electrical discharge machining of nitinol shape memory alloy. *J Mater Res Technol*
- Schneider J et al (2015) Solid state joining of nickel based alloy, Haynes 230. *J Mater Process Technol* 225:492–499
- Nain SS, Garg D, Kumar S (2017) Modeling and optimization of process variables of wire-cut electric discharge machining of super alloy Udimet-L605. *Eng Sci Technol Int J* 20(1):247–264
- Ezugwu E, Wang Z, Machado A (1999) The machinability of nickel-based alloys: a review. *J Mater Process Technol* 86(1–3):1–16
- Martelo D, Morana R, Akid R (2021) Understanding the mechanical behaviour of 718 and 625+ nickel based super-alloys under cathodic polarization. *Theor Appl Fract Mech* 112:102871
- Chaudhari R et al (2021) Pareto optimization of WEDM process parameters for machining a NiTi shape memory alloy using a combined approach of RSM and heat transfer search algorithm. *Adv Manuf* 9(1):64–80
- Chaudhari R et al (2019) Multi-response optimization of WEDM process parameters for machining of superelastic nitinol shape-memory alloy using a heat-transfer search algorithm. *Materials* 12(8):1277
- Kumar V et al (2018) GA-based optimisation using RSM in WEDM of Nimonic-90: a nickel-based super alloy. *Int J Ind Syst Eng* 28(1):53
- Antar M et al (2012) Fatigue response of Udimet 720 following minimum damage wire electrical discharge machining. *Mater Des* 42:295–300
- Li Z et al (2022) Simulation and experiment of ECM accuracy of cooling holes considering the influence of temperature field. *Case Stud Therm Eng* 102112
- Vora J et al (2022) A review on machining aspects of shape memory alloys. *Recent Adv Mech Infrastruct* 449–458
- Ezugwu E, Wang Z (1997) Titanium alloys and their machinability—a review. *J Mater Process Technol* 68(3):262–274
- Fan H et al (2019) An optimization method of upsetting process for homogenized, nickel-based superalloy Udimet 720Li ingot considering both cracking and recrystallization. *J Mater Process Technol* 269:52–64
- Mwangi JW et al (2020) Characterization of the arcing phenomenon in micro-EDM and its effect on key mechanical properties of medical-grade Nitinol. *J Mater Process Technol* 275:116334
- Fuse K et al (2021) Integration of fuzzy AHP and fuzzy TOPSIS methods for wire electric discharge machining of titanium (Ti6Al4V) alloy using RSM. *Materials* 14(23):7408
- Li Z et al (2022) Modeling of two-scale array microstructure and prediction of apparent contact angle based on WEDM. *Int J Adv Manuf Technol*
- Akıncıoğlu S (2022) Taguchi optimization of multiple performance characteristics in the electrical discharge machining of the TiGr2. *Facta Univ Ser Mech Eng* 20(2):237–253
- Vakharia V et al (2022) Experimental investigations and prediction of WEDMed surface of Nitinol SMA using SinGAN and DenseNet deep learning model. *J Mater Res Technol*
- Ishfaq K et al (2021) Minimizing the corner errors (top and bottom) at optimized cutting rate and surface finish during WEDM of Al6061. *Eng Sci Technol Int J* 24(4):1027–1041
- Al-Amin M et al (2021) Multi-objective optimization of process variables for MWCNT-added electro-discharge machining of 316L steel. *Int J Adv Manuf Technol* 1–20
- Phate MR, Toney SB (2019) Modeling and prediction of WEDM performance parameters for Al/SiCp MMC using dimensional analysis and artificial neural network. *Eng Sci Technol Int J* 22(2):468–476
- Philip JT, Mathew J, Kuriachen B (2021) Transition from EDM to PMEDM—impact of suspended particulates in the dielectric on Ti6Al4V and other distinct material surfaces: a review. *J Manuf Process* 64:1105–1142
- Chaudhari R et al (2020) Surface analysis of wire-electrical-discharge-machining-processed shape-memory alloys. *Materials* 13(3):530
- Goyal A et al (2022) Experimental investigation for minimizing circularity and surface roughness under nano graphene mixed dielectric EDM exercising fuzzy-ANFIS approach. *Int J Interact Des Manuf* 1–20
- Ming QY, He LY (1995) Powder-suspension dielectric fluid for EDM. *J Mater Process Technol* 52(1):44–54
- Joshi AY, Joshi AYJH (2019) A systematic review on powder mixed electrical discharge machining 5(12):e02963
- Prihandana GS et al (2014) Application of powder suspended in dielectric fluid for fine finish micro-EDM of Inconel 718. *Int J Adv Manuf Technol* 75(1):599–613
- Mandal P, Mondal SC (2021) Multi-objective optimization of Cu-MWCNT composite electrode in electro discharge machining using MOPSO-TOPSIS. *Measurement* 169:108347
- Jadam T et al (2019) EDM performance of Inconel 718 superalloy: application of multi-walled carbon nanotube (MWCNT) added dielectric media. *J Braz Soc Mech Sci Eng* 41(8):1–20
- Pekturk HY et al (2022) Evaluation of the effect of MWCNT amount and dispersion on bending fatigue properties of non-crimp CFRP composites. *Eng Sci Technol Int J* 34:101081
- Mohammadzadeh Sari M, Noordin M, Brusa E (2013) Role of multi-wall carbon nanotubes on the main parameters of the electrical discharge machining (EDM) process. *Int J Adv Manuf Technol* 68(5):1095–1102
- Ram Prabhu T et al (2018) Multi-objective optimization of EDM process parameters by using passing vehicle search (PVS) algorithm. In *Defect and diffusion forum*. *Trans Tech Publ*
- Parsana S et al (2018) Machining parameter optimization for EDM machining of Mg-RE-Zn-Zr alloy using multi-objective passing vehicle search algorithm. *Arch Civil Mech Eng* 18(3):799–817
- Savsani P, Savsani V (2016) Passing vehicle search (PVS): a novel metaheuristic algorithm. *Appl Math Model* 40(5–6):3951–3978
- Singh H, Garg R (2009) Effects of process parameters on material removal rate in WEDM. *J Achiev Mater Manuf Eng* 32(1):70–74
- Soni H, Sannayellappa N, Rangarasaiah RM (2017) An experimental study of influence of wire electro discharge machining parameters on surface integrity of TiNiCo shape memory alloy. *J Mater Res* 32(16):3100–3108
- Peças P, Henriques E (2008) Effect of the powder concentration and dielectric flow in the surface morphology in electrical discharge machining with powder-mixed dielectric (PMD-EDM). *Int J Adv Manuf Technol* 37(11):1120–1132
- Shabgard M, Khosrozadeh B (2017) Investigation of carbon nanotube added dielectric on the surface characteristics and machining

- performance of Ti–6Al–4V alloy in EDM process. *J Manuf Process* 25:212–219
42. Dresselhaus M et al (2004) Electronic, thermal and mechanical properties of carbon nanotubes. *Philos Trans R Soc London Ser A Math Phys Eng Sci* 362(1823):2065–2098
 43. Izman S et al (2012) Effects of adding multiwalled carbon nanotube into dielectric when EDMing titanium alloy. *Adv Mater Res Trans Tech Publ*
 44. Prabhu S, Vinayagam B (2011) AFM surface investigation of Inconel 825 with multi wall carbon nano tube in electrical discharge machining process using Taguchi analysis. *Arch Civil Mech Eng* 11(1):149–170
 45. Chaudhari R et al (2021) Experimental investigations and optimization of MWCNTs-mixed WEDM process parameters of nitinol shape memory alloy. *J Market Res* 15:2152–2169
 46. Said FM, Gan JY, Sulaiman J (2020) Correlation between response surface methodology and artificial neural network in the prediction of bioactive compounds of unripe *Musa acuminata* peel. *Eng Sci Technol Int J* 23(4):781–787
 47. Hewidy M, El-Taweel T, El-Safty M (2005) Modelling the machining parameters of wire electrical discharge machining of Inconel 601 using RSM. *J Mater Process Technol* 169(2):328–336
 48. Akincioğlu S et al (2020) Taguchi optimization of surface roughness in the turning of Hastelloy C22 super alloy using cryogenically treated ceramic inserts. *Proc Inst Mech Eng C J Mech Eng Sci* 234(19):3826–3836
 49. Puertas I, Luis C, Alvarez L (2004) Analysis of the influence of EDM parameters on surface quality, MRR and EW of WC–Co. *J Mater Process Technol* 153:1026–1032
 50. Vora J et al (2021) Experimental investigations and Pareto optimization of fiber laser cutting process of Ti6Al4V. *Metals* 11(9):1461
 51. Singh MA et al (2020) Identification of wire electrical discharge machinability of SiC sintered using rapid hot pressing technique. *Ceram Int* 46(11):17261–17271
 52. George J et al (2021) Experimental investigation of silicon powder mixed EDM using graphene and CNT nano particle coated electrodes. *Silicon* 13(11):3835–3851
 53. Nguyen H-P, Ngo N-V, Nguyen QT (2021) Optimizing process parameters in edm using low frequency vibration for material removal rate and surface roughness. *J King Saud Univ Eng Sci* 33(4):284–291
 54. Kumar V et al (2017) WEDM of nickel based aerospace alloy: optimization of process parameters and modelling. *Int J Interact Des Manuf* 11(4):917–929
 55. Rouniyar AK, Shandilya P (2022) Effect of machining parameters on surface roughness and white layer during magnetic field assisted powder mixed EDM of AA6061. *Int J Mater Prod Technol* 64(2):121–139
 56. Chaudhari R et al (2022) Multi-response optimization of Al2O3 nanopowder-mixed wire electrical discharge machining process parameters of nitinol shape memory alloy. *Materials* 15(6):2018
 57. Vora J et al (2022) Multi-response optimization and effect of alumina mixed with dielectric fluid on WEDM process of Ti6Al4V. *Recent Adv Mech Infrastruct*. Springer, pp 277–287
 58. Chaudhari R et al (2021) Parametric optimization and effect of nano-graphene mixed dielectric fluid on performance of wire electrical discharge machining process of Ni55. 8Ti shape memory alloy. *Materials* 14(10):2533
 59. Alhodaib A et al (2021) Experimental investigation on silicon powder mixed-EDM of Nimonic-90 superalloy. Volume 11; Issue 11; p.p. 1673.
 60. Aggarwal V et al (2020) Empirical investigations during WEDM of Ni-27Cu-3.15 Al-2Fe-1.5 Mn based superalloy for high temperature corrosion resistance applications. *Materials* 13(16):3470
 61. Patel Gowdru Chandrashekarappa M et al (2021) Experimental analysis and optimization of EDM parameters on HcHcr steel in context with different electrodes and dielectric fluids using hybrid Taguchi-based PCA-utility and critic-utility approaches. *Metals* 11(3):419
 62. Le VT (2021) Influence of processing parameters on surface properties of SKD61 steel processed by powder mixed electrical discharge machining. *J Mater Eng Perform* 30(4):3003–3023
 63. Kumar V, Jangra K (2016) An experimental study on trim cutting operation using metal powder mixed dielectric in WEDM of Nimonic-90. *Int J Ind Eng Comput* 7(1):133–146
 64. Al-Amin M et al (2020) Powder mixed-EDM for potential biomedical applications: a critical review. *Mater Manuf Process* 35(16):1789–1811
 65. Kumar V et al (2018) Surface modification of WC-Co alloy using Al and Si powder through WEDM: a thermal erosion process. *Part Sci Technol* 36(7):878–886

Publisher's Note Springer Nature remains neutral with regard to jurisdictional claims in published maps and institutional affiliations.